An analytical finite element model for predicting three-dimensional tool forces and chip flow

John S. Strenkowski *, Albert J. Shih, Jong-Cherng Lin

Department of Mechanical and Aerospace Engineering, North Carolina State University, Raleigh, NC 27695-7910, USA

Abstract

A model of three-dimensional cutting is developed for predicting tool forces and the chip flow angle. The approach consists of coupling an orthogonal finite element cutting model with an analytical model of three-dimensional cutting. The finite element model is based on an Eulerian approach, which gives excellent agreement with measured tool forces and chip geometries. The analytical model was developed by Usui et al. [ASME J. Engng Indust. 100(1978) 222; 229], in which a minimum energy approach was used to determine the chip flow direction. The model developed by Usui required orthogonal cutting test data to determine the tool forces and chip flow angle. In this paper, a finite element model is used to supply the orthogonal cutting data for Usui's model. With this approach, a predictive model of three-dimensional cutting can be developed that does not require measured data as input. Cutting experiments are described in which good agreement was found between measured and predicted tool forces and chip flow angles for machining of AISI 1020 steel. © 2002 Elsevier Science Ltd. All rights reserved.

Keywords: Finite element modeling; 3D cutting; Chip flow

1. Introduction

Practical machining operations, such as turning, involve cutting tools with two cutting edges and an included nose radius. In three-dimensional cutting, tool forces and the direction of chip flow are influenced by both cutting edges and the tool nose radius. Reliable predictions of cutting forces and chip flow are important for tool and fixture design and estimation of power requirements.

One of the earliest studies of three-dimensional cutting was undertaken by Merchant [3], in which the mechanics of cutting were analyzed for both orthogonal and oblique cutting. Mechant developed an equation for the chip flow angle, which is defined as the angle between a line that is normal to the cutting edge and the direction of chip flow on the tool face. In 1951, Stabler [4] developed a full geometrical analysis in which the chip flow angle was found to be equal to the inclination angle. This is sometimes referred to as Stabler's flow rule. Good agreement with Stabler's flow rule has been found by many workers, including Shaw et al. [5] and Pal and Koenigsberger [6]. As a result, Stabler's rule has been widely accepted as a satisfactory predictor of chip flow direction. Others have proposed that the chip flow angle depends on the rake angle [7] and the cutting speed [8]. Other relationships for the chip flow angle have been proposed by Armarego and Brown [9], which was subsequently verified by Lin and Oxley [10] with cutting tests. An early attempt to predict three-dimensional cutting forces was also reported by Lin and Oxley [10], in which the forces were predicted from the workpiece flow stress measured in a machining test.

In another effort, Lin [11] applied a similar approach in which the shear strength of the chip at the tool–chip interface was treated as a friction factor. The shear strength was expressed as a function of the strain rate and temperature. Good agreement was found between machining experiments on steel and Stabler's chip flow rule.

Conventional turning operations in which cutting occurs along two cutting edges have also been reported. Hu et al. [12] conducted a series of oblique turning tests

---

* Corresponding author. Tel.: +1-919-515-2365; fax: +1-919-515-7968.

E-mail address: ajshih@eos.ncsu.edu (J.-C. Lin).

Nomenclature

A	Area in the shear plane
A_1, A_2	Areas
b	Cutting width
C_s	Side cutting edge angle
C_e	End cutting edge angle
f	Feed rate
F_h	Horizontal cutting force
F_H	Principal component of the cutting force
F_t	Friction force
F_T	Transverse force
F_V	Vertical force
$[F]$	Global external force vector
i	Inclination angle
$[K]$	Global stiffness matrix
N_t	Normal force
Q	Projected area of the cutting cross section
R	Nose radius
t	Undeformed chip thickness
t_1	Depth of cut
$[U]$	Global nodal velocity vector
U_s	Shear energy rate
U_f	Friction energy rate
V	Cutting velocity
V_c	Chip flow velocity
V_s	Chip velocity in the shear plane
α	Penalty factor
α_n	Rake angle
α_e	Effective rake angle
β	Friction angle
$\dot{\varepsilon}_v$	Volume strain rate
$\dot{\bar{\varepsilon}}$	Second variant of the strain rate tensor
ϕ_e	Shear plane angle, angle between the shear plane and cutting velocity
Π	Potential energy
μ	Viscosity
η_c	Chip flow angle
σ_y	Uniaxial shear stress
τ_s	Shear stress in the shear plane

to determine the effect of two cutting edges on the cutting forces and chip flow direction without considering the effect of the nose radius. The first model for two cutting edges was developed by Colwell [13], in which a geometric model of an equivalent cutting edge was established for sharp-nosed tools. The chip flow over the rake face of the tool was assumed to be perpendicular to the major axis of the projected area of the cut. Although tool geometry effects were considered, this method was limited to zero rake and inclination angles.

Young et al. [14] modified the equivalent cutting edge model by assuming that the resultant friction force coincides with the chip flow direction. The chip was treated as a series of independent thin elements for which

Stabler's rule applied, and the resultant friction force was found as the vector sum of the friction force acting on each element. Although the nose radius was included in this model, the rake angle inclination angles were assumed to be zero.

Practical cutting tools have a nose radius that improves not only the surface finish but also the tool's strength and wear characteristics. One of the first models to include the tool nose radius was due to Usui and his co-workers [1,2]. In this work, the chip is treated as a collection of parallel orthogonal slices so that more complicated three-dimensional cutting processes can be simplified as a series of orthogonal analyses. Using orthogonal cutting test data, a minimum energy method was

used to predict chip flow direction and cutting forces. An equivalent cutting edge model was developed for calculating chip flow angle and cutting forces, in which the effects of nose radius and end cutting edges were considered [15]. These models have important practical implications because they incorporate the nose radius, as well as non-zero rake and inclination angles.

Use of the finite element method for simulating a variety of manufacturing processes such as metal forming [16,17] and cutting [18–33] have been well documented. Van Luttervelt et al. [25] and Mackerle [26] have reviewed the use of finite element modeling of machining operations. Lin and Zheng [24] and Lin and Lin [27,28] used an updated Lagrangian method to study oblique cutting. Ceretti et al. [29] used a three-dimensional finite element code to simulate the turning process. A novel approach for simulating the cutting process was developed by Carroll and Strenkowski [19]. This model employed an Eulerian approach in which the grid is spatially fixed. The workpiece is assumed to behave as a viscoplastic material. The model is more accurate and computationally less intensive than an updated Lagrangian approach. The disadvantage is that the final shape of the chip cannot be easily predicted. Strenkowski and Moon [20] improved the model by including a free surface algorithm to determine the final chip geometry. In addition, the cutting forces, stress, strain rate, and temperature distributions in the tool and workpiece were determined.

The Eulerian approach was utilized by Yang [30] to predict chip breaking for groove-type tools. Athavale [31] and Athavale and Strenkowski [32] applied the Eulerian approach for predicting chip breakability for groove and obstruction-type tools based on a material damage criterion. Further extension of the Eulerian cutting model for three-dimensional oblique cutting has been reported by Hsu [33]. However, the model was limited because the tool nose radius was treated as a series of straight edges. Because the tool nose radius can greatly affect cutting forces and surface finish, a more realistic model that includes the tool nose is needed.

Even with the advancement of high speed computers, it is still not practical for detailed modeling of three-dimensional metal cutting using the finite element technique because of significant computational requirements. As an alternative, the approach taken by Usui et al. [1,2] in which three-dimensional cutting is treated as a series of orthogonal slices offers promise as a practical approach for analyzing cutting processes. In this paper, the shortcoming of Usui's approach of requiring orthogonal cutting data is eliminated because this data is provided by an orthogonal finite element cutting model. By coupling these two approaches, a predictive model of three-dimensional cutting can be developed for a wide range of cutting conditions and tool geometries without requiring extensive cutting tests.

2. Finite element cutting model

An Eulerian finite element technique is well suited for modeling steady state cutting processes. In this method, the workpiece and chip flow through a control volume defined by the finite element grid. The chip shape is established by requiring that external boundaries of the chip be coincident with the assumed chip boundaries. Convergence to the correct chip shape can be achieved through successive iterations.

The workpiece material that forms the chip can be treated as a rigid viscoplastic material with a viscosity given by

$$\mu = \frac{\sigma_y}{\sqrt{3}\dot{\bar{\varepsilon}}} \tag{1}$$

where $\dot{\bar{\varepsilon}}$ is the second invariant of the strain rate tensor. This equation is strictly applicable to ideal plasticity, although an additional term can be included to account for work hardening. Plastic flow occurs when the flow stress exceeds the uniaxial yield stress, σ_y. When the flow stress is less than the yield, the strain rate is zero and the viscosity becomes infinite. Therefore to avoid numerical problems, a bound for the viscosity must be supplied.

The finite element equations for viscoplasticity can be derived in terms of nodal velocities. Using a linear isoparametric quadrilateral element, the velocity and strain rate can be expressed in terms of the nodal velocity. For a two-dimensional flow field, the finite element stiffness equations are derived by requiring that the potential energy rate Π be a minimum. For incompressibility, the following constraint equation must be satisfied

$$\dot{\varepsilon}_v = [M]^T[\dot{\varepsilon}] = \dot{\varepsilon}_{xx} + \dot{\varepsilon}_{yy} + \dot{\varepsilon}_{zz} = 0 \tag{2}$$

where $\dot{\varepsilon}_v$ is the volume strain rate. To impose the incompressibility constraint, a penalty function method is utilized. A penalty factor α, which is a large positive number, is used to modify the potential energy as

$$\Pi^* = \Pi + \int_\Omega \alpha\dot{\varepsilon}_v d\Omega \tag{3}$$

The element stiffness matrix is found by minimizing the augmented potential energy. The global stiffness matrix is then derived by assembling each element in the domain to give:

$$[K][U] = [F] \tag{4}$$

where $[K]$, $[U]$, and $[F]$ represent the global stiffness matrix, nodal velocity vector, and external nodal force vector, respectively.

Note that the stiffness matrix contains the penalty factor α. As α becomes larger, the imposed constraint is more nearly satisfied. For nearly incompressible viscopl-

asticity, α becomes a very large number. Ill-conditioning of the coefficient matrix can result, leading to a loss of accuracy in velocity and large errors in the computed stresses. This problem can be remedied by using a reduced and selective integration technique. In this technique, a lower order one-point integration scheme is applied to the dilatational terms in the stiffness matrix, and a two-point scheme is applied to the deviatoric terms.

Once the velocity has been determined, the strain rate and flow stress can be obtained. In addition, the mean angle of friction can be found as the ratio of the mean normal and frictional force components. The friction angle will be needed to determine the chip flow angle and the three-dimensional tool forces.

3. Review of the three-dimensional cutting analysis

An analytical model developed by Usui et al. [1,2] for predicting the chip flow angle and three-dimensional tool forces is first reviewed. The analysis is based on an energy approach in which three-dimensional cutting is approximated as a series of orthogonal slices. Using orthogonal cutting data under equivalent cutting conditions, the chip flow angle and three-dimensional tool forces can be determined for single-point tools with a nose radius.

Consider first the simplest case of a tool with a zero nose radius as shown in Fig. 1. The inclination angle of the main cutting edge is i, the depth of cut is t_1, and the cutting width is b. When $i = 0$, the cutting configuration is orthogonal. The underlying assumption of the model is that a chip is produced by shear forces acting simultaneously in two planes. The main cutting edge CD produces shear in the trapezoidal plane CEFD, while the
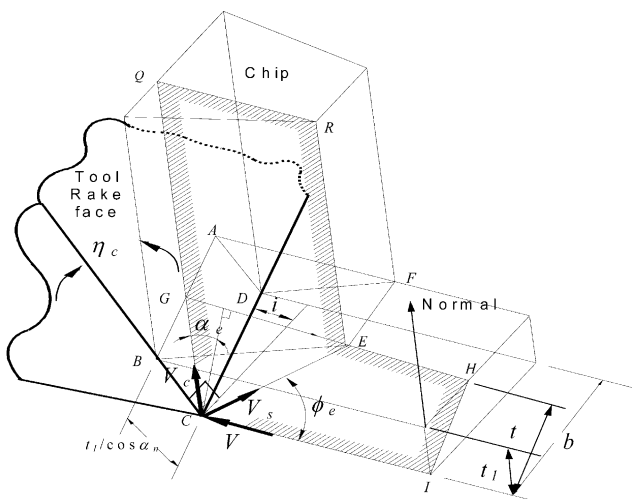

Fig. 1. Basic model of double edge cutting [1] in which the plane IHERQGC represents an orthogonal cutting plane to approximate three-dimensional cutting.

secondary cutting edge CB produces shear in the triangular plane CEB.

In this approach, three-dimensional cutting is simplified as a collection of plane strain orthogonal cutting slices. One typical plane is represented by IHERQGC, which is shown as cross-hatched in Fig. 1. This plane is defined by the cutting velocity V and the chip flow velocity vector V_c. Chip formation in this plane may be regarded as plane strain deformation with a corresponding shear angle, mean friction angle, and work material shear strength as in orthogonal cutting. Therefore, the line CE may be regarded as the shear plane and line HI may be considered the undeformed chip thickness in orthogonal cutting. Any other plane that is parallel to the plane IHERQGC will have the same effective angle and effective rake angle, but it will have a different depth of cut t. Therefore, three-dimensional cutting is interpreted as a series of orthogonal slices, each with the same effective shear angle and effective rake angle along the main cutting edge.

The effective rake angle α_e is measured on the plane which is formed by the chip flow velocity V_c and cutting velocity V, and defined by the angle between the chip flow direction and a line normal to the cutting velocity. This angle can be related to the chip flow angle (η_c), the inclination (i), and the rake (α_n) by [1]

$$\alpha_e = \sin^{-1}(\sin \alpha_n \cos i \cos \eta_c + \sin \eta_c \sin i) \tag{5}$$

The chip flow angle η_c can be determined using an energy approach. The total cutting energy per unit time VF_H, where F_H is the principal component of cutting force, is equal to the consumption of shear energy on the shear plane and friction energy on the tool face. The cutting energy is converted into energy on the shear plane and energy due to friction along the rake face. The energy on the shear plane can be written as an energy rate U_s as [1]

$$U_s = \tau_s V_s A \tag{6}$$

where A is the total shear plane area, and V_s and τ_s are the velocity and shear stress on the shear plane, respectively. The area A consists of the triangle CEB (A_1), and the trapezoid CEFD (A_2) shown in Fig. 1. Usui et al. [1] has shown that the area can be written as explicit functions of the shear angle, inclination angle, effective rake angle, normal rake angle, and chip flow angle. Also from orthogonal theory, the velocity in the shear plane is given by Usui et al. [1]:

$$V_s = \frac{\cos \alpha_e}{\cos(\phi_e - \alpha_e)} V \tag{7}$$

where ϕ_e is the angle between the shear velocity and cutting velocity, and α_e is the effective rake angle. Thus, the shear energy rate U_s in Eq. (6) may be rewritten as [1]:

$$U_{\text{s}} = \frac{\tau_{\text{s}}(A_1 + A_2)\cos\alpha_{\text{e}}}{\cos(\phi_{\text{e}} - \alpha_{\text{e}})}V \qquad (8)$$

The friction energy rate U_{f} on the rake face can be found by a similar analysis [1] as,

$$U_{\text{f}} = F_{\text{t}}\frac{\sin\phi_{\text{e}}}{\cos(\phi_{\text{e}} - \alpha_{\text{e}})}V \qquad (9)$$

In order to calculate the total energy rate from Eqs. (8) and (9), the effective shear plane angle (ϕ_{e}) and the shear plane stress (τ_{s}) must be known. It is assumed that the relationships between ϕ_{e} and τ_{s} and the effective rake angle α_{e} are the same as those in orthogonal cutting under equivalent conditions. In addition, by assuming that the friction force acting on the unit width of the tool face with undeformed chip thickness t is the same as the friction force in orthogonal cutting with unit width of cut and undeformed chip thickness t, the friction force F_{t} can be written as [1]:

$$F_{\text{t}} = \frac{\tau_{\text{s}}\sin\beta\cos\alpha_{\text{e}}}{\cos(\phi_{\text{e}} + \beta - \alpha_{\text{e}})\sin\phi_{\text{e}}}Q \qquad (10)$$

where β is the friction angle on the tool face and Q is given for a sharp tool to be:

$$Q = \frac{bt_1}{\cos i \cos\alpha_{\text{n}}} \qquad (11)$$

These equations can be used to evaluate the friction energy rate U_{f} in Eq. (9).

The total cutting energy can be found by adding the contributions from the shear and friction energy rates. Note that the energy rates are dependent on the chip flow angle η_{c}, which is not known. However, the angle can be found from the condition that the chip will flow in a direction that minimizes the cutting energy U.

The principal tool force F_{H} can be derived from equilibrium of energy to be [1]:

$$F_{\text{H}} = \left\{\frac{\tau_{\text{s}}\cos\alpha_{\text{e}}}{\cos(\phi_{\text{e}} - \alpha_{\text{e}})}\left[(A_1 + A_2)\right.\right. \qquad (12)$$

$$\left.\left. + \frac{bt_1\sin\beta}{\cos(\phi_{\text{e}} + \beta - \alpha_{\text{e}})\cos i \cos\alpha_{\text{n}}}\right]\right\}$$

The normal force N_{t} can be determined from the equation [1]:

$$N_{\text{t}}\cos\alpha_{\text{n}}\cos i + F_{\text{t}}\sin\alpha_{\text{e}} = F_{\text{H}} \qquad (13)$$

Once N_{t} is known, the vertical force F_{V} and transverse force F_{T} components can be written in terms of the normal force N_{t} as [1]:

$$F_{\text{V}} = -N_{\text{t}}\sin\alpha_{\text{n}} + F_{\text{t}}\cos\eta_{\text{c}}\cos\alpha_{\text{n}} \qquad (14)$$

$$F_{\text{T}} = -N_{\text{t}}\cos\alpha_{\text{n}}\sin i + F_{\text{t}}\sin\eta_{\text{c}}\cos i \qquad (15)$$

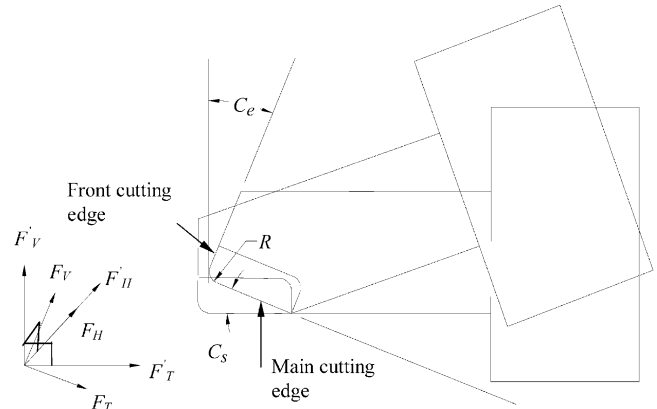$$-F_{\text{t}}\cos\eta_{\text{c}}\sin i \sin\alpha_{\text{n}}$$

Fig. 2. Single point tool with side and end cutting edge angles [2].

where F_{t} is the friction force. Note that in Usui's analysis [1,2], orthogonal cutting tests are necessary to provide the shear stress τ_{s}, shear angle ϕ_{e}, and friction angle β needed in the above equations. The force components are functions of α_{n}, i, b, t_1, and η_{c}. For any cutting condition, the parameters α_{n}, i, b, and t_1 are known constants, while the chip flow angle η_{c} can be evaluated using the energy method. Therefore, the three-dimensional tool forces can be readily determined.

3.1. Tools with nonzero nose radius

A similar energy approach can be taken for predicting the chip flow angle and tool forces for the more general case of a nonzero tool nose radius R as shown in Fig. 2, where C_{s} is the side cutting edge angle and C_{e} is the end cutting edge angle [2].

Consider a tool for which the nose radius R is large compared to the feed rate f, as shown in Fig. 3. Following the same procedure as for a zero nose radius tool, expressions for U_{s} and U_{f} can be derived [2]:
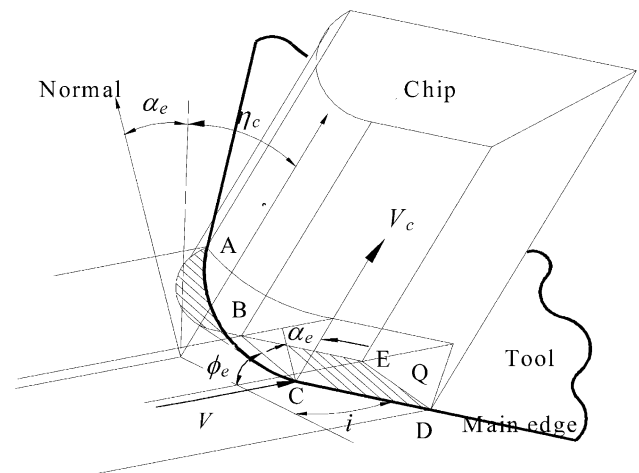

Fig. 3. Shear plane and projected area Q of cutting cross section for tool with large nose radius as compared with feed rate [2].

$$U_s = \tau_s A V_s = \frac{\tau_s A \cos \alpha_e}{\cos(\phi_e - \alpha_e)} V \qquad (16)$$

$$U_f = F_t V_c = \frac{\tau_s \sin \beta \cos \alpha_e}{\cos(\phi_e + \beta - \alpha_e)\cos(\phi_e - \alpha_e)} QV \qquad (17)$$

where A is the area of the shear plane, and Q is the projected area of the cutting cross section to the tool face in the cutting velocity V direction. Note that Q depends on the tool nose radius and it is different in general than the value given in Eq. (11). The shear plane can be divided into several sections depending on the tool face geometry and cutting conditions. Three types of cutting cross-sections can be identified, depending on whether the nose radius R is less than, equal to, or greater than the depth of cut.

Using geometrical considerations, relationships for A and Q in terms of η_c, ϕ_e, α_e, the tool geometry, and the cutting conditions can be found [2]. The chip flow angle η_c and the three-dimensional tool forces are found by minimizing the energy. Other tools in which the nose radius R is smaller than the feed rate can also be addressed with this approach, as described by Usui and Hirota [2].

3.2. The finite element model

Isoparametric quadrilateral finite elements with four nodes and eight degrees-of-freedom were used to model the workpiece and tool. A sample finite element mesh that represents orthogonal cutting under plane strain conditions with a 5° rake angle, 11° clearance angle, and 0.762 mm depth of cut is shown in Fig. 4. A finer mesh is used in areas in which high stress gradients occur, such as the shear zone along the rake face of the cutting tool and the primary shear zone. Different meshes with a similar configuration were used to simulate other rake angles and depth of cuts.
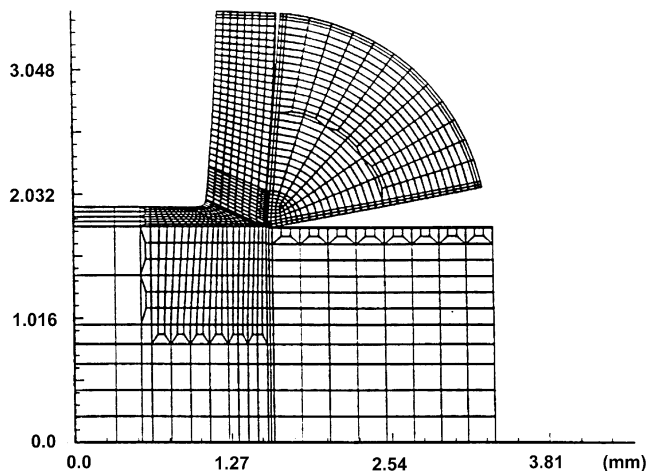
4. Coupling finite element and analytical models

In Usui's original three-dimensional analysis [1,2], orthogonal cutting tests were conducted to provide the necessary data for the analytical model. This data consists of the shear stress on the shear plane τ_s, the friction angle β, and the shear plane angle ϕ_e. Note that the relationship between ϕ_e and α_e is assumed to be the same as that for ϕ and α for the equivalent orthogonal cutting conditions. In this paper, the input data consisting of τ_s, β, and ϕ_e is derived from the finite element orthogonal cutting model. The computed shear stress τ_s varied linearly from 568 MPa for a zero rake angle to 548 MPa for a 20° rake for AISI 1020 steel. Fig. 5 shows the computed friction and shear plane angles for several rake angles. The friction angle β is found from the vertical and principal force components, which are also computed with the finite element model. Finally, the shear plane angle ϕ_e is derived from the computed chip geometry as the slope of a line between a maximum nodal strain rate and a node on the cutting edge of the tool. Note that the shape and thickness of the chip is iteratively determined with the finite element model. The chip shape is adjusted until the velocity along its boundaries is completely tangential to the free surfaces of the chip. Using this criterion for convergence, the chip thickness was usually found within twenty iterations.

The advantage of using the finite element model instead of orthogonal cutting experiments is that data can be obtained more readily than from cutting tests. In addition, tool shapes other than flat tools with sharp edges can be simulated. For example, the finite element model allows for the introduction of a radius on the cutting edge. Other tool shapes can also be simulated, such as groove and obstruction type tools. Note that care must be exercised in applying this theory to tools other than sharp flat tools because many of the underlying equa-

Fig. 4. A sample two-dimensional finite element mesh for 0.762 mm depth of cut, 5° rake angle, and 11° clearance angle.
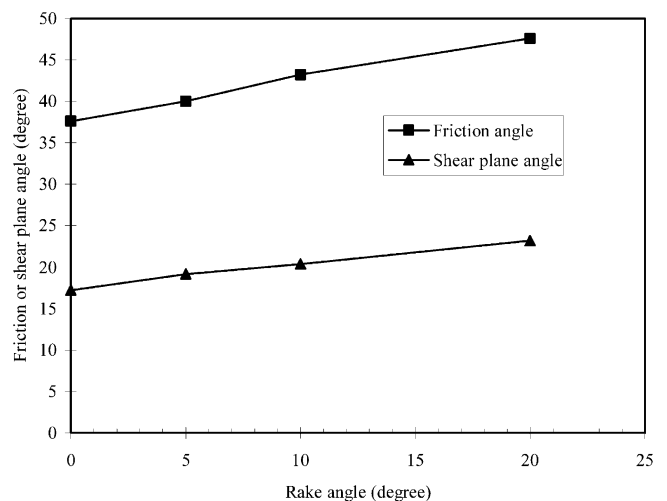

Fig. 5. Predicted orthogonal friction and shear plane angles for AISI 1020 (depth of cut=0.76 mm, feed=0.165 mm/rev, speed=1.6 m/s).

tions used in the analytical cutting model are applicable only to sharp flat tools. Nonetheless, the procedure developed in this paper provides the foundation for the study of more advanced tools for three-dimensional cutting.

5. Experimental setup

Cutting experiments were conducted to validate the three-dimensional cutting model. A low carbon AISI 1020 steel seamless tube, 38.1 mm in diameter and 9.53 mm thick, was used as the workpiece. The cutting experiments were conducted on a 3.7 kW conventional lathe. Flat commercial carbide tool inserts TPG-3 series with four nose radii ranging from 0.4 to 1.59 mm were used to machine the steel workpiece for speeds of 1.2 and 1.6 m/s, inclination angles from 0 to 15°, and feed rates of 0.09 and 0.165 mm/rev. The TPG-3 series cutting tools were triangular KC 810 carbide inserts produced by Kennametal.

For tools with more than one cutting edge, the chip flow angle η_c was determined by measuring wear marks on the tool. Photographs of the tools were prepared with a metallographic microscope and the orientation of the score marks was measured with a toolmaker's microscope. The principal, vertical, and transverse force components were measured using a Kistler 3198 piezoelectric dynamometer mounted on the traversing carriage of the lathe. Two cutting tests were performed for each cutting condition and the average of the two measurements was recorded as the final result.

6. Validation of the cutting model

The three-dimensional cutting analysis was validated by comparing predicted chip flow angles and tool forces with cutting test data. The measured and predicted chip flow angles are compared in Fig. 6 for an inclination
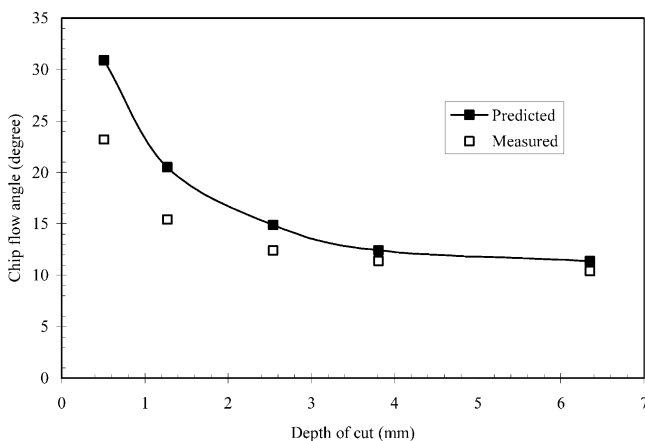
angle of 10° for a flat tool with a nose radius of 0.79 mm and a feed of 0.165 mm/rev. Similar agreement was found for an inclination angle of 5° for the same tool and cutting conditions, as well as for a slower cutting speed of 1.2 m/s. As expected, the chip flow angle approaches the inclination angle for large depths of cut, which is consistent with Stabler's rule. This is because as the depth of cut becomes large, the main cutting edge dominates the cutting process and the end cutting edge only plays a minor role. Note that measurement accuracy of the chip flow angle is diminished somewhat for small depths of cut because the chip is highly flexible at these depths of cut.

A comparison between the predicted and measured tool force components is shown in Fig. 7, in which the forces are shown as a function of the tool nose radius. The cutting conditions for these forces were a depth of cut of 0.76 mm, a speed of 1.6 m/s, and a feed rate of 0.165 mm/rev. In general, the principal cutting force is nearly constant, while the vertical force decreases with tool radius. In contrast, the transverse force increases with the tool radius. This is consistent with the observation that the chip flow angle increases with tool radius. This is expected because a larger radius tool will engage a greater portion of the workpiece, thus increasing both the transverse force and the chip flow angle. Similar cutting tests were undertaken for other conditions, including a slower cutting speed of 1.2 m/s and a larger depth of cut of 1.9 mm. Good agreement was found with an average discrepancy of about 15%.

Figure 8 shows the variation of the three tool force components with inclination angle for the TPG-322 flat tool with a nose radius of 0.79 mm, feed of 0.165 mm/rev, speed of 1.2 m/s, and depth of cut of 1.52 mm. Excellent agreement was found between measured and predicted forces. Similar agreement was found for tools

Fig. 6. Comparison of predicted and measured chip flow angle versus depth of cut ($i = 10°$, feed=0.165 mm/rev, speed=1.6 m/s).
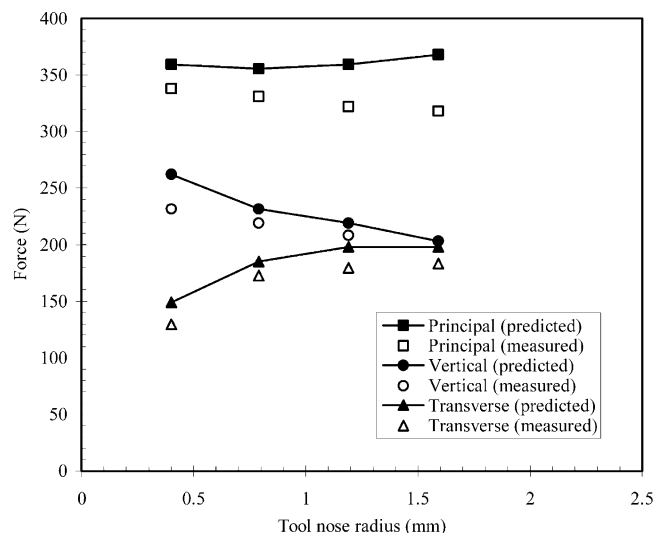

Fig. 7. Comparison of the tool forces versus nose radius (feed=0.165 mm/rev, speed=1.6 m/s, depth of cut=0.76 mm).
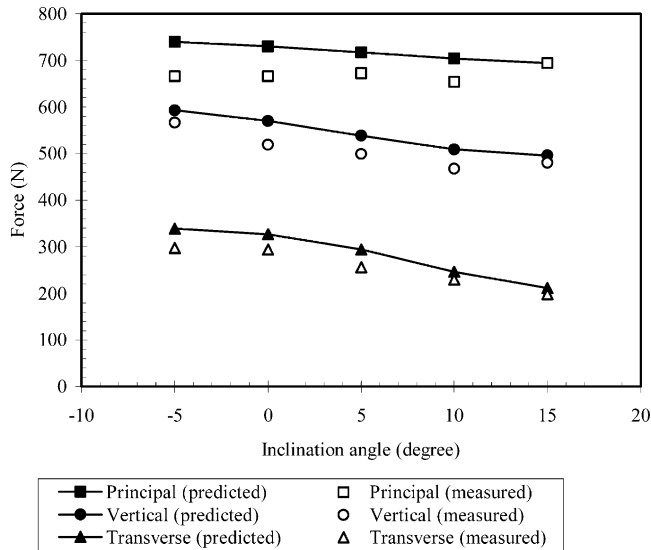
Fig. 8. Comparison of tool forces versus inclination angle (feed=0.165 mm/rev, speed=1.2 m/s, depth of cut=1.52 mm).

with different nose radii of 0.4, 1.19, and 1.59 mm, operating at a speed of 1.6 m/s for depths of cut of 0.76 and 1.9 mm.

The model developed by Usui et al. [1,2] treated the tool as sharp. In reality, all tools have a slight rounding of the cutting edge for strength. An average edge radius of 0.05 mm was measured for the tools in this paper. The edge radius becomes more significant as the feed rate is reduced, because deformation in the primary shear zone is more highly effected by the cutting edge radius. Therefore, less agreement between the measured and predicted tool forces would be anticipated for smaller feed rates. This can be seen in Fig. 9 for a tool with a
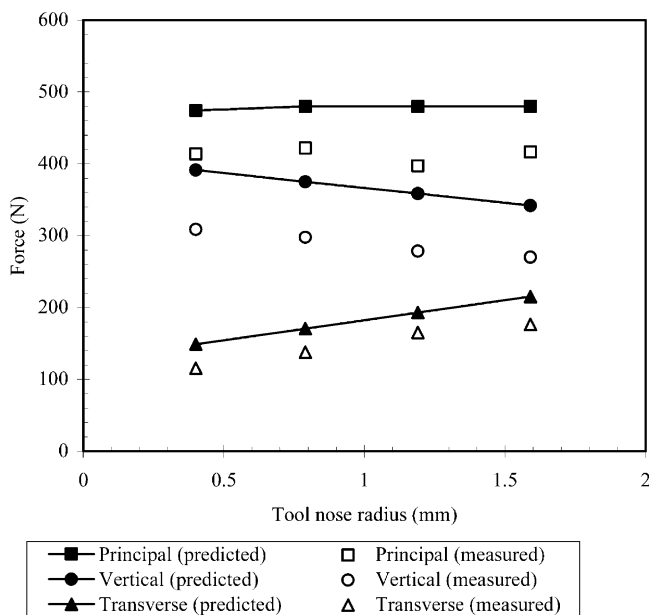
feed of 0.09 mm/rev. In contrast, the discrepancy between measured and predicted tool forces is much smaller when cutting under comparable conditions but with a larger feed of 0.165 mm/rev, as shown in Fig. 10.

7. Conclusions

In this paper, an analytical model of three-dimensional cutting developed by Usui et al. [1,2] is coupled with an Eulerian finite element model of orthogonal cutting. In the original analytical model, the three-dimensional cutting process was treated as a collection of equivalent orthogonal slices. Data for each slice was derived from orthogonal cutting tests. In this paper, a finite element cutting model is used to provide the input data, which consists of the shear angle, the shear stress acting on the shear plane, and the friction angle.

Several flat tools with different nose radii were tested under a variety of cutting conditions to verify the model. Very good agreement was found based upon measured three-dimensional tool forces and chip flow angles. It was also found that although the model developed by Usui et al. [1,2] is strictly applicable to only sharp flat tools, the model can be used for tools with a cutting edge radius if the feed rate is sufficiently large as compared to the edge radius. Therefore, good agreement between measured and predicted forces and chip flow angles was found for these tools provided that the feed rate is large compared to the cutting edge radius.

The advantage of this approach is that three-dimensional tool forces and chip flow angles can be predicted without the need for corresponding cutting tests. In

Fig. 9. Comparison of the tool forces versus nose radius (feed=0.09 mm/rev, speed=1.6 m/s, depth of cut=1.9 mm).
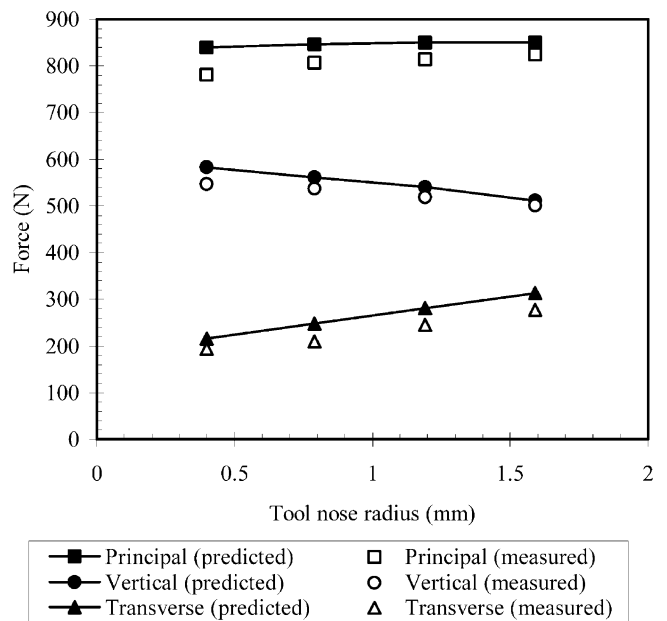

Fig. 10. Comparison of the tool forces versus nose radius (feed=0.165 mm/rev, speed=1.6 m/s, depth of cut=1.9 mm).

addition, more complex tool geometries such as groove-type chipbreaker tools can be analyzed. Therefore, a true predictive model of cutting can be achieved for studying a wide range of cutting conditions and tool geometries prior to fabrication, thereby reducing design time and development costs for new and more complex tool geometries.

References

[1] E. Usui, M. Hirota, A. Masuko, Analytical prediction of three dimensional cutting process: part 1 basic cutting model and energy approach, ASME Journal of Engineering for Industry 100 (1978) 222–228.

[2] E. Usui, A. Hirota, Analytical prediction of three dimensional cutting process: part 2 chip formation and cutting force with conventional single-point tool, ASME Journal of Engineering for Industry 100 (1978) 229–235.

[3] M.E. Mechant, Basic mechanics of the metal cutting process, ASME Journal of Applied Mechanics 11 (1944) 168–175.

[4] G.V. Stabler, The fundamental geometry of cutting tools, Proceedings of the Institution of Mechanical Engineers 165 (1951) 14–26.

[5] M.C. Shaw, N.H. Cook, P.A. Smith, The mechanics of three-dimensional cutting operations, Transactions of the ASME 74 (1952) 1055–1064.

[6] A.K. Pal, F. Koenigsberger, Some aspects of the oblique cutting process, International Journal of Machine Tool Design and Research 8 (1968) 45–57.

[7] J.K. Russell, R.H. Brown, The measurement of chip flow direction, International Journal of Machine Tool Design and Research 6 (1966) 129–138.

[8] N.N. Zorev, Metal Cutting Mechanics, Pergamon Press, Oxford, 1966.

[9] E.J.A. Armarego, R.H. Brown, The Machining of Metals, Prentice-Hall, Englewood Cliffs, NJ, 1969.

[10] G.C.I. Lin, P.L.B. Oxley, Mechanics of oblique machining: predicting chip geometry and cutting forces from work material properties and cutting conditions, Proceedings of the Institution of Mechanical Engineers 186 (1972) 813–820.

[11] G.C.I. Lin, Prediction of cutting forces and chip geometry in oblique machining from flow stress properties and cutting conditions, International Journal of Machine Tool Design and Research 18 (1978) 117–130.

[12] R.S. Hu, P. Mathew, P.L.B. Oxley, Allowing for end cutting edge effects in predicting forces in bar turning with oblique machining conditions, Proceedings of the Institution of Mechanical Engineers 200 (C2) (1986) 89–99.

[13] L.V. Colwell, Predicting the angle of chip flow for single-point cutting tools, Transactions of the ASME 76 (1954) 199–204.

[14] H.T. Young, P. Mathew, P.L.B. Oxley, Allowing for nose radius effects in predicting the chip flow direction and cutting forces in bar turning, Proceedings of the Institution of Mechanical Engineers. 201 (C3) (1987) 213–226.

[15] J. Wang, P. Mathew, Development of a general tool model for turning operations based on a variable flow stress theory, International Journal of Machine Tools and Manufacture 35 (1995) 71–90.

[16] O.C. Zienkiewicz, P.N. Godbole, Flow of plastic and visco-plastic solids with special reference to extrusion and forming processes, International Journal for Numerical Methods in Engineering 8 (1974) 3–16.

[17] A.J. Shih, H.T. Yang, Experimental and finite element simulation methods for rate-dependent metal forming processes, International Journal for Numerical Methods in Engineering 31 (1991) 345–367.

[18] J.S. Strenkowski, J.T. Carroll III, A finite element model of orthogonal metal cutting, ASME Journal of Engineering for Industry 107 (1985) 349–354.

[19] J.T. Carroll III, J.S. Strenkowski, Finite element models of orthogonal cutting with application to single point diamond turning, International Journal of Mechanical Sciences 30 (1988) 899–920.

[20] J.S. Strenkowski, K.J. Moon, Finite element prediction of chip geometry and tool/workpiece temperature distributions in orthogonal metal cutting, ASME Journal of Engineering for Industry 112 (1990) 313–318.

[21] A.J. Shih, Finite element simulation of orthogonal metal cutting, ASME Journal of Engineering for Industry 117 (1995) 84–93.

[22] R. Ghosh, O.W. Dillon, I.S. Jawahir, An investigation of 3-D curled chip in machining—part 1: a mechanics-based analytical model, Machining Science and Technology 2 (1) (1998) 91–116.

[23] R. Ghosh, O.W. Dillon, I.S. Jawahir, An investigation of 3-D curled chip in machining—part 2: simulation and validation using FE techniques, Machining Science and Technology 2 (1) (1998) 117–145.

[24] Z.C. Lin, Y.L. Zheng, Study on the thermo-elastic-plastic cutting model for 3-D tool with chip breaker, ASME Journal of Engineering Materials and Technology 120 (1998) 265–274.

[25] C.A. van Luttervelt, T.H.C. Childs, I.S. Jawahir, F. Klocke, P.K. Venuvinod, Present situation and future trends in modeling of machining operations. Progress report of the CIRP working group 'modeling of machining operations', CIRP Annals 47 (2) (1998) 587–626.

[26] J. Mackerle, Finite-element analysis and simulation of machining: a bibliography (1976–1996), Journal of Materials Processing Technology 86 (1999) 17–44.

[27] Z.C. Lin, Y.Y. Lin, Fundamental modeling for oblique cutting by thermo-elastic-plastic FEM, International Journal of Mechanical Sciences 41 (1999) 941–965.

[28] Z.C. Lin, Y.Y. Lin, A study of an oblique cutting model, Journal of Materials Processing Technology 86 (1999) 119–130.

[29] E. Ceretti, C. Lazzaroni, L. Menegardo, T. Altan, Turning simulations using a three-dimensional FEM code, Journal of Materials Processing Technology 98 (2000) 99–103.

[30] J.A. Yang, A predictive model of chip breaking for groove-type tools in orthogonal machining of AISI 1020 steel, Ph.D. dissertation, North Carolina State University (1992).

[31] S.M. Athavale, A damage-based model for predicting chip breakability for obstruction and groove tools, Ph.D. dissertation, North Carolina State University (1994).

[32] S.M. Athavale, J.S. Strenkowski, Material damage-based model for predicting chip-breakability, Journal of Manufacturing Science and Engineering 119 (11) (1997) 675–680.

[33] J.M. Hsu, A three-dimensional finite element model of metal cutting, Ph.D. dissertation, North Carolina State University (1990).